Earth and Planetary Science Letters 449 (2016) 360–371

Contents lists available at ScienceDirect

Earth and Planetary Science Letters

www.elsevier.com/locate/epsl

On the iron isotope composition of Mars and volatile depletion in the terrestrial planets

Paolo A. Sossi [a,*], Oliver Nebel [a,b], Mahesh Anand [c,d], Franck Poitrasson [e]

[a] Research School of Earth Sciences, Australian National University, Canberra 2601, ACT, Australia
[b] School of Earth, Atmosphere and Environment, Monash University, Melbourne 3800, VIC, Australia
[c] Department of Physical Sciences, Open University, Milton Keynes, MK76AA, UK
[d] Department of Earth Sciences, The Natural History Museum, London, SW7 5BD, UK
[e] Laboratoire Géosciences Environnement Toulouse, CNRS UMR 5563 – UPS – IRD, 14-16, Avenue Edouard Belin, 31400, Toulouse, France

ARTICLE INFO

Article history:
Received 4 December 2015
Received in revised form 14 May 2016
Accepted 21 May 2016
Available online 8 June 2016
Editor: B. Marty

Keywords:
Mars
Fe isotopes
petrogenesis
SNC
accretion
volatile depletion

ABSTRACT

Iron is the most abundant multivalent element in planetary reservoirs, meaning its isotope composition (expressed as δ^{57}Fe) may record signatures of processes that occurred during the formation and subsequent differentiation of the terrestrial planets. Chondritic meteorites, putative constituents of the planets and remnants of undifferentiated inner solar system bodies, have $\delta^{57}\text{Fe} \approx 0‰$; an isotopic signature shared with the Martian Shergottite–Nakhlite–Chassignite (SNC) suite of meteorites. The silicate Earth and Moon, as represented by basaltic rocks, are distinctly heavier, $\delta^{57}\text{Fe} \approx +0.1‰$. However, some authors have recently argued, on the basis of iron isotope measurements of abyssal peridotites, that the composition of the Earth's mantle is $\delta^{57}\text{Fe} = +0.04 \pm 0.04‰$, indistinguishable from the mean Martian value. To provide a more robust estimate for Mars, we present new high-precision iron isotope data on 17 SNC meteorites and 5 mineral separates. We find that the iron isotope compositions of Martian meteorites reflect igneous processes, with nakhlites and evolved shergottites displaying heavier $\delta^{57}\text{Fe}(+0.05 \pm 0.03‰)$, whereas MgO-rich rocks are lighter ($\delta^{57}\text{Fe} \approx -0.01 \pm 0.02‰$). These systematics are controlled by the fractionation of olivine and pyroxene, attested to by the lighter isotope composition of pyroxene compared to whole rock nakhlites. Extrapolation of the δ^{57}Fe SNC liquid line of descent to a putative Martian mantle yields a δ^{57}Fe value lighter than its terrestrial counterpart, but indistinguishable from chondrites. Iron isotopes in planetary basalts of the inner solar system correlate positively with Fe/Mn and silicon isotopes. While Mars and IV-Vesta are undepleted in iron and accordingly have chondritic δ^{57}Fe, the Earth experienced volatile depletion at low (1300 K) temperatures, likely at an early stage in the solar nebula, whereas additional post-nebular Fe loss is possible for the Moon and angrites.

1. Introduction

How planets in the inner solar system accreted and differentiated is a question fundamental to understanding the chemical differences that exist between them today. Iron offers a unique opportunity to address this question. Not only is it abundant in each of the major planetary reservoirs, the crust, mantle and core, it exists in three different oxidation states – Fe^{3+}, Fe^{2+} and Fe^0 – the relative proportions of which are constrained by local redox conditions. These redox states confer different properties to the element, making it capable of tracing a variety of processes.

Despite the range of iron oxidation states, its isotopes are remarkably constant in chondritic meteorites, identical to the IRMM-014 reference material (Schoenberg and von Blanckenburg, 2006; Craddock and Dauphas, 2011; Needham et al., 2009; Theis et al., 2008; Wang et al., 2013); i.e., $((^{57}\text{Fe}/^{54}\text{Fe})_{\text{chondrite}}/(^{57}\text{Fe}/^{54}\text{Fe})_{\text{IRMM-014}} - 1)*1000 = \delta^{57}\text{Fe} = 0‰$. This constancy is independent of chondrite class, thus, if planets accreted from chondritic material, deviations from 0‰ should reflect post-nebular processes. Mass-dependent fractionation laws dictate that, in general, Fe^{3+}-bearing phases are heavier than Fe^{2+}-bearing phases, i.e., $\delta Fe^{3+} - \delta Fe^{2+} = \Delta Fe^{3+-2+} > 0‰$ (Polyakov and Mineev, 2000; Shahar et al., 2008), although no apparent isotopic fractionation exists between Fe^{2+} and Fe^0 under terrestrial core-forming conditions (Hin et al., 2012; Poitrasson et al., 2009; Roskosz et al., 2006).

* Corresponding author at: Institut de Physique du Globe de Paris, Sorbonne Paris Cité, Université Paris Diderot, CNRS, F-75005 Paris, France.
E-mail address: sossi@ipgp.fr (P.A. Sossi).

http://dx.doi.org/10.1016/j.epsl.2016.05.030

Using this behaviour as a guide, causes for isotopic differences in basaltic rocks from different planetary bodies can be evaluated. Initial studies considered that δ^{57}Fe in the BSE ≈0.1‰, owing to the overlap of ultramafic to intermediate magmatic rocks, (Beard and Johnson, 2004; Poitrasson et al., 2004). This signature is also observed in the lunar low-Ti basalts (Liu et al., 2010; Poitrasson et al., 2004; Weyer et al., 2005), whereas the lunar high-Ti basalts are systematically enriched in δ^{57}Fe (≈0.2‰). Iron isotope signatures for the Earth–Moon system, based on basaltic rocks, are resolvably heavier than estimates for SNC meteorites (Anand et al., 2006; Poitrasson et al., 2004; Wang et al., 2012; Weyer et al., 2005) and the Howardite–Eucrite–Diogenite rocks from asteroid IV-Vesta (Poitrasson et al., 2004; Schoenberg and von Blanckenburg, 2006; Wang et al., 2012; Weyer et al., 2005), both of which give chondritic values. Further, the recognition of basaltic achondrites extending to even heavier values than those of the Earth–Moon system (i.e., angrites, ≈0.2‰) suggests heavy isotope enrichment is a consequence of planetary differentiation. Possible explanations include vaporisation and loss of isotopically-light Fe during planetary collisions (Poitrasson et al., 2004), isotope fractionation during mantle partial melting (Dauphas et al., 2009; Weyer and Ionov, 2007) and fractionation by high-pressure phases in the lower mantle during core formation (Polyakov, 2009; Williams et al., 2012).

However, and while not widely agreed upon (see, e.g., Zhao et al., 2012; Poitrasson et al., 2013) some recent studies on the composition of mantle peridotites (Craddock et al., 2013; Weyer and Ionov, 2007) suggest a BSE value that is lighter (δ^{57}Fe ≈ 0.04 ± 0.04‰) than mean values for terrestrial and lunar basalts, as represented by Mid-Ocean Ridge Basalt, MORB (δ^{57}Fe ≈ 0.1‰; Teng et al., 2013) and the low-Ti suite, respectively. Importantly, this value is similar to chondrites, Mars and IV-Vesta, removing the need to appeal to fractionation mechanisms between Earth and these bodies. In order to shed light on the isotopic characteristics of Mars, we have analysed 17 whole-rock SNC meteorites and 5 mineral separates using high-precision techniques (Poitrasson and Freydier, 2005; Sossi et al., 2015). Through identification of the primary and parental magma compositions of SNCs, and applying corrections for the effects of magmatic differentiation, the iron isotopic composition of Martian primary magmas is calculated and shown to be lighter than that of primary MORB, meaning the Martian and terrestrial mantles are isotopically distinct. A comparison of planetary basalts shows a systematic dependence on Fe/Mn ratios, implying a common process leading to iron isotope fractionation. Mass balance constrains the transfer of material to be significant on the planetary-scale, namely by volatile depletion or core-formation. We interpret these results in the context of the accretion and differentiation histories of the terrestrial planets.

2. Samples and methods

2.1. Samples and dissolution

Samples Shergotty, Zagami, Los Angeles, SaU 005, NWA 1183, Nakhla, Governador Valadares, Lafayette and Chassigny were provided by the Natural History Museum, London. Samples Y 980459 and Y 000953 were obtained from the National Institute for Polar Research, Japan. The Australian National University samples DaG 476 and Zagami were purchased from a meteorite dealer, whereas samples ALHA 77005, EETA 79001A, LAR 06319, RBT 4262 and MIL 03346 were provided by the Meteorite Working Group (MWG), NASA, in the form of 1 g rock chips, free of fusion crusts. Exactly 500 mg of these chips was hand-crushed in a boron carbide mortar and pestle to create a fine powder. Of this batch, 100 mg was dissolved in duplicate for the stable isotope analyses, first by a mixture of concentrated HCl–HF–HNO_3 in the ratio 1:0.5:0.2 in a 3 mL Savillex Teflon beaker on a table-top hotplate set to ≈130 °C. After drying down in nitrate form, 15 M HNO_3 with a few drops of HF were added to the samples and then placed, still in their 3 mL Teflon beaker, inside 20 mL FEP Teflon vessels with 2–3 mL of MQ H_2O to create a vapour pressure, and inserted into steel bombs. These were left to dissolve in an oven set to ≈210 °C for 7 days. Subsequent evaporation with addition of concentrated HNO_3 confirmed that the samples had been dissolved in their entirety.

2.2. Column chromatography and mass spectrometry

Samples were analysed in two batches – those marked 'Poitrasson' were processed at Geosciences Environnement Toulouse (GET) CNRS laboratory, following the procedure detailed in Poitrasson and Freydier (2005). Owing to the reproducibility of data acquired during multiple sessions over the period, standard-sample bracketing (SSB) results were used rather than the combined SSB and Ni-doped regression method of Poitrasson and Freydier (2005). Samples labelled 'Sossi' were analysed at the Australian National University, following the procedure described in Sossi et al. (2015). Three well-characterised standard materials, Allende, BHVO-2 and Milhas Hematite were run throughout to ensure total procedural accuracy and precision were maintained (Table 1) in agreement with published values (Sossi et al., 2015).

3. Results

Iron isotope measurements for the SNC meteorites are summarised in Table 1. Whole-rock major- and trace-element data and literature iron isotope data are listed in Appendix A.

The iron isotope compositions of whole rocks show a restricted range, $-0.07 \pm 0.01 < \delta^{57}\text{Fe}(‰) < +0.10 \pm 0.03$, overlapping with those of both chondrites and mantle peridotites. Measured δ^{57}Fe values are inversely correlated with whole-rock MgO contents (Fig. 1a), mimicking trends observed in terrestrial mafic rocks (Sossi et al., 2012; Teng et al., 2008). Within the shergottites, a similar correlation is found with iron isotopes and CaO (Fig. 1b), with the nakhlites displaced towards higher CaO values as a result of clinopyroxene accumulation. Similar systematics are observed when compared with other indices of magmatic differentiation, such as Ni, Sc and modal olivine content (Fig. 1c). Individual analyses compare favourably with other recent measurements (shown in grey, Fig. 1), and most notably with recent high precision measurements (Wang et al., 2012). For meteorites analysed in both studies ($n = 7$), a correlation coefficient of 0.6 is observed, respectable considering the limited isotopic range (0.15‰) compared to analytical uncertainty (0.03–0.05‰). This argues against any significant sample heterogeneity or bias in analytical methods, such that values reported herein can be interpreted with confidence.

Although based on a smaller dataset ($n = 5$), pyroxene (from nakhlites) and olivine (from Chassigny) separates define an even narrower spread than the whole rocks, extending from $\delta^{57}\text{Fe} = -0.04 \pm 0.05$‰ to $+0.05 \pm 0.06$‰. Calculated pyroxene–whole rock fractionation factors are resolvable in the Y 000593 and Lafayette nakhlites, where $\Delta^{57}\text{Fe}_{\text{px-nak}} = -0.08 \pm 0.01$‰ and -0.07 ± 0.05‰, respectively (Fig. 1d). Pyroxene–nakhlite pairs from Nakhla and MIL 03346 show no resolvable difference, a result mirrored by the olivine–chassigny pair (Fig. 1d).

4. Discussion

4.1. Petrogenesis of Martian SNCs

In attempting to link the geochemistry and iron isotope compositions of SNC meteorites to that of the Martian mantle and terrestrial rocks, estimates of parental magma compositions are required. On the basis of geochemical criteria, Martian basalts are derived

Table 1
Iron isotopic compositions of SNC whole rocks, mineral separates and standards.

	Method	δ^{57}Fe (‰)	2 SE	δ^{56}Fe (‰)	2 SE	*n*
Whole rocks						
Shergottites						
ALHA 77005	Sossi Ni Spike	−0.068	0.009	−0.042	0.006	4
RBT 4262	Sossi Ni Spike	0.006	0.001	0.003	0.004	4
EETA 79001A	Sossi Ni Spike	−0.014	0.042	−0.011	0.026	4
LAR 06319	Sossi Ni Spike	−0.027	0.054	−0.019	0.040	4
Shergotty	Poitrasson SSB	0.033	0.060	0.016	0.047	6
Zagami	Combined	0.095	0.031	0.055	0.030	8
Los Angeles	Poitrasson SSB	0.045	0.010	0.027	0.019	6
Y980459	Poitrasson SSB	0.057	0.014	0.022	0.037	9
DaG 476	Combined	0.011	0.007	0.016	0.013	8
SaU 005	Poitrasson SSB	0.007	0.016	0.010	0.038	6
NWA 1183	Poitrasson SSB	0.043	0.002	0.013	0.012	6
Nakhlites						
MIL 03346	Combined	0.077	0.043	0.046	0.023	12
Nakhla	Poitrasson SSB	0.009	0.029	0.010	0.003	6
Governador Valadares	Poitrasson SSB	0.044	0.016	0.022	0.019	6
Y000593	Poitrasson SSB	0.093	0.008	0.056	0.032	6
Lafayette	Poitrasson SSB	0.031	0.027	0.024	0.066	6
Chassignites						
Chassigny	Poitrasson SSB	0.024	0.001	0.007	0.038	6
Mineral separates						
Nakhla Px	Poitrasson SSB	−0.006	0.040	−0.009	0.003	6
MIL 03346 Px	Poitrasson SSB	0.047	0.058	0.023	0.011	6
Y000593 Px	Poitrasson SSB	0.009	0.000	0.003	0.001	6
Lafayette Px	Poitrasson SSB	−0.038	0.047	−0.032	0.045	6
Chassigny Ol	Poitrasson SSB	0.037	0.060	0.014	0.014	6
Standards						
BHVO-2	Sossi Ni Spike	0.155	0.031	0.107	0.051	2
Allende	Sossi Ni Spike	0.001	0.028	0.001	0.032	2
Hematite	Poitrasson SSB	0.753	0.094	0.514	0.049	48

Note: SSB: sample and standard bracketing mass bias correction and Ni-doping uses natural Ni isotope composition to correct for mass bias. See text, Poitrasson and Freydier, 2005, and Sossi et al., 2015 for analytical details.
n: number of individual MC-ICP-MS measurements.

from disparate sources: 'depleted', 'intermediate' and 'enriched' (Blichert-Toft et al., 1999; Borg and Draper, 2003; Herd et al., 2002; Jones, 1989). As a result, a single parental magma for the SNC meteorites is untenable. Rather, the degree to which each whole-rock composition is representative of a liquid can be estimated through mineral–liquid equilibria. Of these, the best-constrained is the $K_{D\ \mathrm{Ol\text{–}Melt}}^{\mathrm{Fe\text{–}Mg}}$ (Filiberto and Dasgupta, 2011; Roeder and Emslie, 1970; Toplis, 2005), and, as olivine is present in both the mantle, and as the liquidus phase in basaltic melts, it is also the most useful mineral for this purpose.

Olivines in Martian shergottites display extensive normal zoning, where Mg# decreases from core to rim (Shearer et al., 2013, 2008), complicating identification of the earliest-crystallised olivine. This uncertainty can be mitigated by assuming that the most magnesian olivine composition, which corresponds to the core of the crystal, is the first to crystallise (provided it is not xenocrystic; Wadhwa et al., 2001). Its forsterite content may be compared with the Mg# of the melt with which it would have been in equilibrium, according to the expressions of Toplis (2005), and Filiberto and Dasgupta (2011). Toplis (2005) showed that the $K_{D\ \mathrm{Ol\text{–}Melt}}^{\mathrm{Fe\text{–}Mg}}$ is sensitive to melt composition, and specifically its SiO_2 content. For Martian melt compositions, a blanket value of 0.35 is applicable according to Filiberto and Dasgupta (2011), in agreement with the Toplis (2005) expression, which predicts 0.33 for shergottite–olivine pairs, both of which are higher than canonical $K_{D\ \mathrm{Ol\text{–}Melt}}^{\mathrm{Fe\text{–}Mg}} \approx 0.3$. Applying these equilibrium constants, samples that have olivines in equilibrium with the whole-rock, and therefore approximate liquids, are EETA 79001A, Y 980459 and slightly adcumulate LAR 06319 (Fig. 2a). Given the same $K_D^{\mathrm{Fe\text{–}Mg}}$ for pyroxene–melt (Bédard, 2010; von Seckendorff and O'Neill, 1993), the Shergotty and Los Angeles shergottites are close to (albeit more evolved) melt compositions (Fig. 2b). Assuming the forsterite content is fixed, the vertical departure from the equilibrium lines in Figs. 2a and 2b yields the fraction of mineral accumulation by mass balance:

$$M_{\mathrm{Eq}} = \frac{M_{\mathrm{WR}} - M_{\mathrm{Min}} * f_{\mathrm{Min}}}{(1 - f_{\mathrm{Min}})}, \tag{1}$$

which describes the concentration of an oxide or element, M, (here, MgO or FeO) in the melt (Eq) in equilibrium with the most magnesian mineral, Min (either olivine or pyroxene). The subscript WR denotes the whole rock, and f is the fraction, where $0 < f < 1$. f is fixed by the constraint that:

$$\frac{(\mathrm{Fe_{Min}}/\mathrm{Mg_{Min}})}{(\mathrm{Fe_{Eq}}/\mathrm{Mg_{Eq}})} = 0.35 \tag{2}$$

As a result, the MgO and FeO contents of the parental melts for each sample are also obtained. A summary of these calculations is presented in Table 2. In general, the amount of accumulation compares well with the observed modal abundances – for example, equation (1) predicts 92% accumulation of Fo_{68} olivine to create Chassigny, compared with the 91.6% determined petrographically (Prinz et al., 1974).

4.2. Primary melts and the Fe/Mg ratio of the Martian mantle

Correction of a given melt composition along an olivine control line (a vertical trajectory) until it reaches the curve in Fig. 2a gives the composition of the parental liquid. However, the identity of the primary magma, that is, one in equilibrium with its

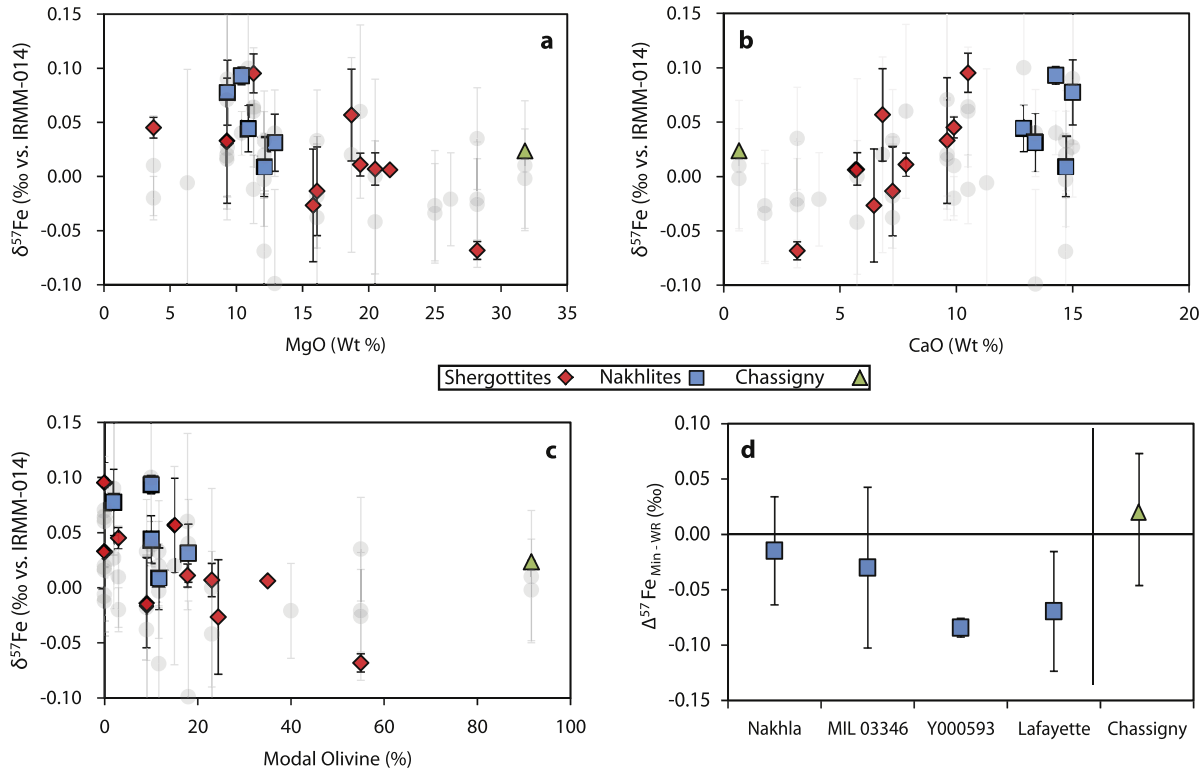

Fig. 1. The iron isotopic composition of whole-rock Shergottites (red diamonds), Nakhlites (blue squares) and Chassigny (green triangle) meteorites plotted against their a) MgO (wt%), b) CaO (wt%) and c) modal olivine contents. Literature data is shown in grey circles, from Poitrasson et al. (2004), Weyer et al. (2005), Anand et al. (2006) and Wang et al. (2012). d) Fractionation factors between pyroxene (nakhlites) and olivine (Chassigny) with the whole rock. Uncertainties are shown at the 2σ levels. (For interpretation of the references to colour in this figure legend, the reader is referred to the web version of this article.)

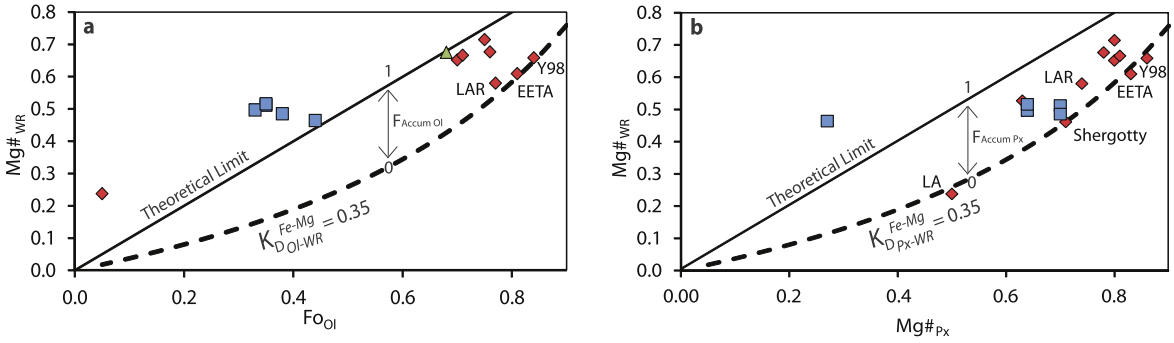

Fig. 2. The amount of a) olivine and b) pyroxene accumulation calculated for whole-rock compositions, assuming a $K_{D\ \mathrm{Min-Liq}}^{\mathrm{Fe-Mg}} = 0.35$. Samples plotting on the dashed lines resemble liquid compositions, where increasing vertical departure from the equilibrium curve is proportional to the fraction of the accumulated mineral, where the theoretical limit is $\mathrm{Mg\#_{WR}} = \mathrm{Mg\#_{Min}}$.

mantle source, can be determined only by making assumptions as to the Martian mantle composition. For this purpose, we adopt a mantle with ≈30 wt% MgO and 17–18 wt% FeO (see Taylor, 2013, and Wanke and Dreibus, 1988 for summaries). Together, they suggest a $\mathrm{Mg\#_{Mantle-Mars}} = 0.75$–$0.77$, significantly more iron-rich and magnesium-poor than its terrestrial counterpart ($\mathrm{Mg\#_{Mantle-Earth}} = 0.89$; Palme and O'Neill, 2014). Therefore, applying a $K_{D\ \mathrm{Ol-Melt}}^{\mathrm{Fe-Mg}} = 0.33$ to 0.35, primary Martian melts will have Mg#s between 0.5 and 0.55, depending on the extent of melting and choice of $K_{D\ \mathrm{Ol-Melt}}^{\mathrm{Fe-Mg}}$. Whether this condition has been met is illustrated graphically (Fig. 3), showing the melt compositions from Table 2.

The presence of olivines with Mg#s ≥0.77 in some shergottites (EETA 79001A, 0.81; Liu et al., 2013, Y 980459, 0.84; Usui et al., 2008) highlights a mismatch between their sources and a putative mantle composition. There are several possible explanations for such a discrepancy:

1. The Mg# of the Martian mantle is higher than 0.77
2. The Martian mantle is heterogeneous, voiding the assumption of a value common to all SNCs
3. The Mg# of the residual mantle changes substantially with degree of partial melting

The estimated Mg# varies little between Martian compositional models (option 1), as Mg, which is lithophile during core formation (O'Neill et al., 1998; Ringwood and Hibberson, 1991), is well-constrained. Iron contents are known less precisely due to uncertainty in the composition of the Martian core (Taylor, 2013; Wanke and Dreibus, 1988). Additionally, the Martian mantle composition may vary with depth (option 2). Crystallisation of a Martian magma ocean would have led to an initially mineralogically-stratified mantle (Borg and Draper, 2003; Elkins-Tanton et al., 2003), where the Mg# decreased rapidly towards the upper 200 km of the Martian mantle by accumulation

Table 2
Results of Fe–Mg equilibria calculations between whole rocks and ferromagnesian minerals, and the iron isotope composition of parental magma, assuming $\Delta^{57}Fe_{Min\text{-}Melt} = -0.1‰$ (Section 4.3).

Whole rocks	Measured			Calculated					
	Fo	Mg# Px	Mg# WR	MgO (wt%) parent	FeO (wt%) parent	Mg# parent	Accum. Ol	Accum. Px	δ^{57}Fe (‰) parent
Shergottites									
ALHA 77005	0.75	0.80	0.714	8.8	14.8	0.515	0.65	–	0.006
RBT 4262	0.70	0.80	0.651	6.2	13.4	0.450	0.53	–	0.076
EETA 79001A	0.81	0.83	0.609	15.4	18.4	0.599	0.03	–	−0.011
LAR 06319	0.77	0.74	0.580	13.4	20.3	0.541	0.09	–	−0.017
Shergotty	–	0.71	0.461	7.4	19.4	0.405	–	0.10	0.043
Zagami	–	0.63	0.527	3.9	14.4	0.324	–	0.40	0.147
Los Angeles	0.05	0.50	0.238	4.3	21.8	0.259	–	0.00	0.039
Y980459	0.84	0.86	0.658	17.6	17.1	0.647	0.05	–	0.063
DaG 476	0.76	0.78	0.676	8.6	13.5	0.532	0.35	–	0.058
SaU 005	0.74	0.81	0.666	8.3	14.5	0.505	0.41	–	0.060
Nakhlites									
MIL 03346	0.44	0.27	0.464	5.0	32.6	0.214	0.58	–	0.106
Nakhla	0.35	0.70	0.512	11.9	26.0	0.449	–	0.33	0.024
Governador Valadares	0.33	0.64	0.497	9.7	27.7	0.383	–	0.44	0.065
Y000593	0.38	0.70	0.485	9.9	22.2	0.442	–	0.20	0.103
Lafayette	0.35	0.64	0.516	13.5	38.3	0.386	–	0.58	0.057
Chassignites									
Chassigny	0.68	–	0.675	5.3	12.4	0.436	0.92	–	0.120

Data sources for measured values are listed in Appendix A.

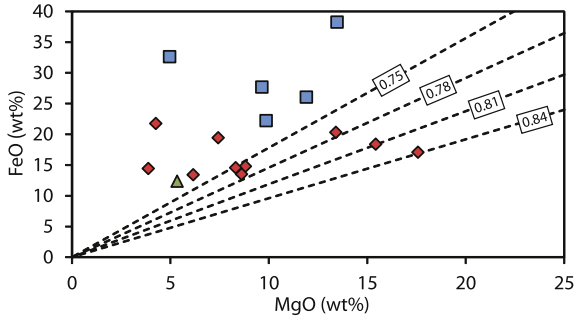

Fig. 3. FeO–MgO systematics of SNC liquids, that is, whole rocks after correction for olivine or pyroxene accumulation (Section 4.2; Table 2). Dashed lines show the Mg# of the residual mantle with which the melts would be in equilibrium. Melts in equilibrium with mantle with Mg# $\geq$ 0.75 are considered primary liquids.

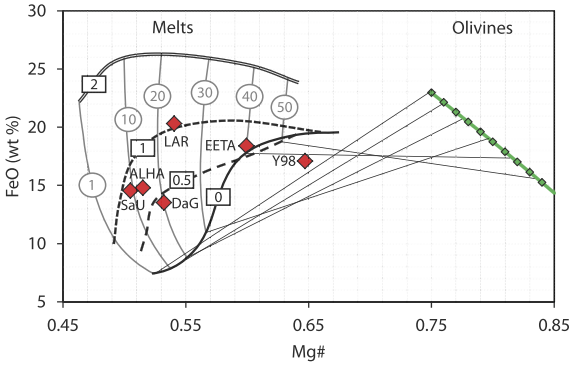

Fig. 4. Calculated primary melt compositions of Martian magmas (red diamonds, see Table 2), overlain by curves from alphaMELTS modelling (Section 4.2). Black lines and numbers in boxes refer to isobars, ranging between 10^{-4} GPa (labelled "0") and 2 GPa, while grey lines and numbers in circles represent percentages of partial melting. Tie lines connect degrees of partial melting at 0 GPa with the olivine Mg# of the residual mantle (green diamonds). (For interpretation of the references to colour in this figure legend, the reader is referred to the web version of this article.)

of olivine and pyroxene at the base. Subsequently, this unstable density configuration might have prompted mantle overturn, acting to re-distribute and homogenise its major element composition, though the lower temperatures than on Earth may have inhibited convection and homogenisation of the mantle such that distinct reservoirs could have survived (Elkins-Tanton et al., 2005). The preservation of characteristic REE and isotopic signatures in SNC groups (Borg and Draper, 2003; Bridges and Warren, 2006; Halliday et al., 2001) point to the diversity of mantle source compositions.

In addition to, and independent of mantle heterogeneity, the increase in Mg# of residual mantle with melt extraction (option 3) is a fundamental result of Fe–Mg partitioning between ferromagnesian minerals and melt. To model the extent of this Mg# change, and to compare the partial melts to those calculated for the primary shergottite magmas (Table 2), the *alphaMELTS* algorithm (Smith and Asimow, 2005) was used. Equilibrium melting was simulated through incremental isobaric heating of the Dreibus and Wanke (1985) mantle estimate at 1 bar, 0.5, 1, and 2 GPa, at FMQ-2 (Fig. 4). At a given melt fraction (F), higher pressure (P) melts contain both more MgO and FeO. This phenomenon is due to the expansion of the pyroxene stability field at the expense of olivine to higher pressures, such that olivine enters the melt more readily. As these phases have similar Mg#s, that of the melt varies little with P, rendering it a powerful indicator of F.

The Fe–Mg systematics of primary shergottite melts suggest formation by 10–25% melting at pressures between 0.5 and 1 GPa (≈40–85 km; Fig. 4). These pressures and melt fractions are also in-line with their SiO_2 contents of ≈50 wt%, whose behaviour is again a function of the proportion of olivine (low SiO_2; high F, P) to pyroxene (high SiO_2; low F, P). For the same source, the more mafic primary melts calculated for EETA79001A and Y 980459 give correspondingly higher melt fractions; 40% and >50% respectively. Notably, sample Y 980459 plots at a FeO content too low (or MgO too high) to have been produced from melting of a mantle envisaged by Dreibus and Wanke (1985), even at 1 bar, suggestive of a more magnesian source region (Khan and Connolly, 2008; Musselwhite et al., 2006).

4.3. Iron isotope fractionation during magmatic processes and the effect of oxygen fugacity

Even though the SNCs potentially come from diverse sources (Section 4.2), whether this variation begets a change in iron isotope composition is crucial in understanding the composition of the Martian mantle. On Earth, it has been suggested that frac-

tional crystallisation and perhaps partial melting produce iron isotope fractionation in minerals and melts (Dauphas et al., 2009; Sossi et al., 2012; Teng et al., 2008). The driving force behind this fractionation is the contrasting redox and structural states of iron between the two phases, imparting different vibrational energies on the Fe–O bond by virtue of changing bond stiffness. The stiffer bonds of Fe^{3+}, which typically exists in tetrahedral co-ordination, concentrates the heavier isotopes over the larger, octahedrally-co-ordinated Fe^{2+} ion (Schauble, 2004).

However, before these equilibrium systematics can be applied, the extent of kinetic (i.e., disequilibrium) fractionation must be evaluated. Physically, kinetic fractionation can develop in response to crystals attempting to equilibrate with changing melt composition, since isotopes have differential diffusivities. In terrestrial systems, significant iron isotope fractionation occurs during iron diffusion into Mg-rich olivines, manifest as strong negative departures (up to 2‰) from equilibrium values in minerals (Oeser et al., 2015; Sio et al., 2013). However, nakhlites record no kinetic iron isotope fractionation within the analytical uncertainty of ±0.5‰, even in instances were diffusive processes are evidenced by Mg isotopes (Sio et al., 2014), likely reflecting their high Fe contents. Although normal zoning is common in Martian ferromagnesian minerals, zoning caused by fractional crystallisation, where each zone reflects local equilibrium with the coexisting melt, does not produce any additional isotope fractionation. Textural analysis (Richter et al., 2016) suggests that diffusive zoning arose after the bulk of the rock had already crystallised. Thus, diffusive re-equilibration took place in a closed system, affecting only the internal mineral–melt isotope distribution and not the bulk rock. Furthermore, diffusion-produced zones, volumetrically, comprise but a small fraction of the mineral (10–50 μm; Richter et al., 2016), and hence should not contribute significantly to its composition, though Fe–Mg zoning in shergottites can be more extensive. Therefore, more precise *in-situ* measurements are required to better evaluate the effect of diffusive processes. On current evidence, however, mineral pairs should record equilibrium partitioning, a point underlined by the small measured fractionation factors, which are ≈0‰ or slightly negative (Fig. 1d). Should these negative values arise from diffusion, they should depend on nakhlite cooling rates, where MIL > Y000593 > Nakhla = GV > Lafayette (fastest to slowest; Day et al., 2006) in which the fastest cooled magmas would have the largest isotope fractionation among minerals, for which there is no evidence. Therefore, the discussion that follows makes the reasonable assumption that equilibrium conditions prevailed during SNC petrogenesis.

Olivine, as the first phase to crystallise upon shallow-level differentiation of mafic and ultramafic melts of both Martian (Musselwhite et al., 2006) and terrestrial (Arndt, 1976) melt compositions, incorporates $^{VI}Fe^{2+}$ but not Fe^{3+}, thereby having lower $Fe^{3+}/\Sigma Fe$ than the coexisting liquid. Martian magmas, which crystallise between FMQ-3.5 to FMQ-1, that is IW-0.5 to +2 (Herd, 2003; Herd et al., 2002; Wadhwa, 2008, 2001), have $Fe^{3+}/\Sigma Fe$ between 0.02–0.07 (Righter et al., 2013), lower than terrestrial magmas, but higher than olivine (≈0). Given the higher oxidation state of terrestrial basalts, where $Fe^{3+}/\Sigma Fe$ of MORB = 0.12 (Bézos and Humler, 2005), the Fe isotopic fractionation factor between olivine and melt should be larger (Dauphas et al., 2014; Dauphas et al., 2009; Wang et al., 2012), that is, $\Delta^{57}Fe^{FMQ-3}_{Ol\text{-}Melt} < \Delta^{57}Fe^{FMQ}_{Ol\text{-}Melt}$. Enrichment of heavy iron isotopes in the melt by ferromagnesian silicate crystallisation is documented for various localities on Earth (Teng et al., 2008; Sossi et al., 2012; Chen et al., 2014). Taking terrestrial igneous rocks as a whole, heavy $\delta^{57}Fe$ only becomes pronounced in granitic compositions (e.g. Poitrasson and Freydier, 2005). Although many Martian meteorites are partial cumulates, a first-order constraint on the magnitude of the isotopic fractionation may be attempted by comparing the evolution of $\delta^{57}Fe$ with the MgO content of the whole rock as a proxy for the liquid (Fig. 5).

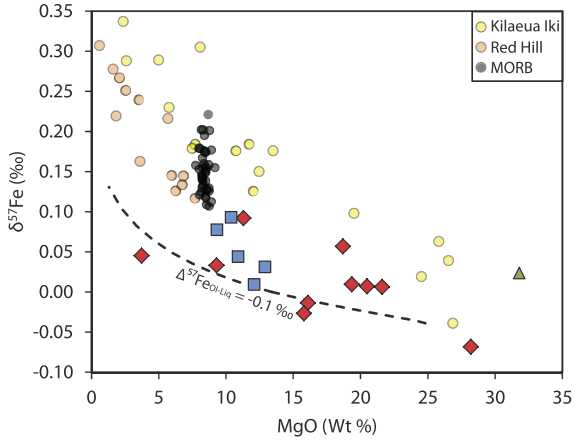

Fig. 5. Iron isotope compositions of SNC meteorites (symbols as per Fig. 1) as a function of MgO content. Plotted for comparison are terrestrial tholeiitic magmas from Kilauea Iki (Teng et al., 2008), Red Hill (Sossi et al., 2012) and MORB (Teng et al., 2013). The black dashed line represents the evolution of a parent magma with 13.5 wt% MgO and $\delta^{57}Fe = 0$‰ by fractional crystallisation and olivine accumulation for a $\Delta^{57}Fe_{Ol-Melt} = -0.1$‰.

Two notable features of the $\delta^{57}Fe$–MgO systematics are revealed: 1. The slope of the array is smaller in Martian compositions; 2. Magmas from Earth are displaced towards higher $\delta^{57}Fe$ at a given MgO content. The data of Teng et al., 2008 predicts a $\Delta^{57}Fe_{Min-Melt} = -0.15$‰, as do the magmas of the Red Hill intrusion (Sossi et al., 2012). The greater scatter of the Martian magmas notwithstanding, the trend may be fitted by $\Delta^{57}Fe_{Min-Melt} = -0.10$‰, an approximation considering that Martian shergottites have experienced varying polythermal cooling histories (Basu Sarbadhikari et al., 2009; Goodrich, 2003) and some of the samples are partially accumulative (see Section 4.1). Generally, however, the degree of fractionation is smaller than on Earth. Lunar basalts, which contain exclusively Fe^{2+}, show no dependence of $\delta^{57}Fe$ with indices of differentiation (Liu et al., 2010), suggesting that Fe^{3+}/Fe^{2+}_{melt} exerts control on the magnitude of iron isotope fractionation. For a given composition, $Fe^{3+}/\Sigma Fe$ scales linearly with the mean Fe–O bond strength (quantified by the force constant; Dauphas et al., 2014), hence, for Martian basalts with half as much Fe^{3+} compared to terrestrial tholeiitic basalts, the fractionation factor is commensurately halved, in-line with observations (Fig. 5).

The recognition of the smaller fractionation factor between ferromagnesian minerals and Martian melts indicates that, should iron isotope fractionation during melting occur, it would be smaller. Indeed, the magnitude of this effect is limited on Earth ($\delta^{57}Fe$ decreases ≤ 0.1‰ in peridotites that record partial melting; Poitrasson et al., 2013). Therefore, if the variation in Martian source composition is produced by prior melt extraction as suggested by their REE patterns (e.g. Borg and Draper, 2003), $\delta^{57}Fe$ should be little affected, if at all.

4.4. Iron isotope compositions of primary magmas on Mars

In order to facilitate comparison between planetary basalts, iron isotopes must be corrected for the effects of crystal fractionation (Section 4.3) until the whole rock composition approximates that of a liquid. To perform this correction, we adopt $\Delta^{57}Fe_{Ol\text{-}Melt} \approx -0.1$‰, as derived in Section 4.3. A change of ±0.05‰ in the fractionation factor makes little difference, particularly at high Mg#s where the whole rocks are already close to liquids (Fig. 5). Furthermore, these more primitive examples, with 0.5 < Mg# <0.65 are the most suitable for constraining the iron isotope composition of the Martian mantle.

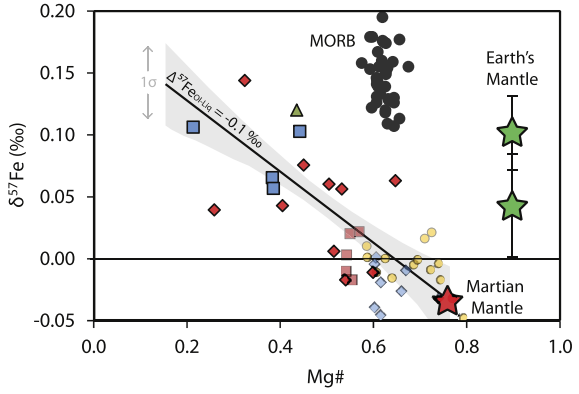

Fig. 6. Iron isotope compositions of SNCs corrected for olivine/pyroxene accumulation assuming a $\Delta^{57}Fe_{Min\text{-}Melt} = -0.1$ ‰ (black line). The Martian array, including associated 1σ uncertainty (grey envelope) is lighter than MORB (black circles) and the Earth's primitive mantle (green stars) at a given Mg#, leading to a mantle composition (red star) within uncertainty of chondrites. Chondrites: Enstatite = red squares, Carbonaceous = blue diamonds, Ordinary = yellow circles; iron isotope data from Needham et al. (2009); Poitrasson et al. (2004); Schoenberg and von Blanckenburg (2006), and Craddock and Dauphas (2011), MgO values from Jarosewich (1990). (For interpretation of the references to colour in this figure legend, the reader is referred to the web version of this article.)

Following correction, Martian liquids define a trend of increasing δ^{57}Fe with decreasing Mg# (Fig. 6) similar to that in Fig. 5. Melts with Mg#s near 0.6 have $\delta^{57}Fe \approx 0$‰, whereas the more evolved shergottites and nakhlite liquids (Mg# <0.5) preserve corrected δ^{57}Fe near 0.05‰. Extrapolation of this trend to the Mg# of the Martian mantle (0.77) yields a value of -0.04 ± 0.03‰ (1SD). The majority of the uncertainty at Mg# = 0.77 comes from the scatter in the array (±0.025‰), with minor effects from the choice of fractionation factor (±0.005‰ for a 0.05‰ change in $\Delta^{57}Fe_{Min\text{-}Melt}$), and the composition of the Martian mantle (±0.002‰ per 0.01 change in Mg#). This value is lighter than that of the Earth's mantle based on abyssal peridotites ($+0.04 \pm 0.04$‰; Craddock et al., 2013), at the 1SD level, though indistinguishable at 2SD, and therefore distinction between them is limited by the precision of the technique. Other estimates for the Earth's mantle are resolvably heavier, however, including those derived from continental xenoliths (+0.1‰; Poitrasson et al., 2013) and terrestrial basalts ($+0.10 \pm 0.03$‰; Poitrasson, 2007; Poitrasson et al., 2004).

Owing to the isotopic scatter in terrestrial peridotites, isotopic differences between the Earth and Mars are better resolved by basaltic rocks (Fig. 5). Mid-Ocean Ridge Basalts, the most abundant magmas currently produced on Earth, have $0.57 < Mg\# < 0.68$ (Jenner and O'Neill, 2012), with a mean of 0.62 ± 0.02 (1 SD), assuming 12% Fe^{3+} (Bézos and Humler, 2005). At a given Mg#, MORBs are ≈0.1‰ heavier in δ^{57}Fe than Martian shergottites, a relationship that holds for Hawaiian basalts and other tholeiitic magmas (Fig. 5). This difference outweighs the effect of increased isotope fractionation during partial melting on Earth, which would account for ≈0.03‰ (Dauphas et al., 2014). Therefore, if the SNC meteorites are a suitable analogue for Martian volcanism, then the Martian mantle is resolvably lighter than that of its terrestrial counterpart.

5. Contrasted accretion of the terrestrial planets

5.1. A comparison of basaltic rocks

To better understand processes operating at the planetary scale, basalts are preferred over a hypothetical mantle, since no unambiguous records of planetary mantles exist. Three caveats apply; firstly, fractional crystallisation of Fe–Mg minerals has a small effect on the iron isotope compositions of planetary magmas, depending on the redox state, where $\Delta^{57}Fe_{Min\text{-}Melt} \approx 0.15$‰ = Earth (FMQ) > Mars > Moon (IW-1) = 0‰ (Section 4.3). In the same vein, partial melting causes enrichment of heavy iron in partial melts relative to sources, though this effect is smaller compared with fractional crystallisation, owing to the higher temperatures, $\Delta^{57}Fe_{Min\text{-}Melt} \approx 0.05$‰ = Earth (FMQ) > Mars > Moon (IW-1) = 0‰ (Section 4.3). Finally, we assume that basalts are representative of the body, which may not be the case (see Section 4.2).

To mitigate bias arising from these uncertainties, primitive (high Mg#) basalts are selected. The 'Mean Mafic Earth', $\delta^{57}Fe = +0.10 \pm 0.03$‰ (Poitrasson et al., 2013) is assumed for the Earth, whereas near-primary shergottites give $\delta^{57}Fe = -0.01 \pm 0.02$‰, for Mars. For smaller bodies, low-Ti basalts were chosen to better represent the composition of the Moon, as high-Ti basalts have ilmenite in their source regions (caveat 3, e.g. Green et al., 1975). Similarly, the main trend Eucrites (as opposed to Stannern or Nuevo Laredo trend) were selected, owing to their higher Mg#s and lower TiO_2 contents (Barrat et al., 2000). The limited number of angrite meteorites constrains an average to be taken from Wang et al. (2012), yielding $+0.19 \pm 0.02$‰. An average of the ureilite analyses of Barrat et al. (2015), 0.08 ± 0.03‰, is also represented, even though these are phaneritic, ultramafic partial melting residua.

Iron isotopes in basaltic rocks of inner solar system bodies show a more protracted range than chondrites, extending exclusively to heavier compositions. Only processes that involve a significant mass transfer of Fe, and/or are associated with a large isotope fractionation, can shift its composition on the planetary-scale. These constraints may be satisfied by i) core formation (e.g. Williams et al., 2012) and ii) volatile depletion (e.g., Poitrasson et al., 2004). In discerning between these two commonly invoked modes of fractionation, the Fe/Mn ratio is particularly useful. Manganese behaves like iron geochemically during magma petrogenesis (Davis et al., 2013) such that Fe/Mn remains roughly constant during partial melting and fractional crystallisation (Qin and Humayun, 2008). It does, however, differ in two important ways from Fe under conditions relevant to planet formation; Mn is more volatile and also far less siderophile. The Fe/Mn ratio in planetary basalts shows an excellent positive correlation with their iron isotope compositions (Fig. 7). In the following sections, possible mechanisms giving rise to this trend are explored.

5.2. Core formation

Though planetary bodies possess metallic cores, whether their formation, at disparate P, T, X and fO_2 (Rai and van Westrenen, 2013; Righter and Drake, 1996; Rubie and Jacobson, 2015) causes iron isotope fractionation in the complementary mantle is uncertain. Despite this complexity, equilibrium isotope fractionation is subject to a $1/T^2$ dependence, therefore, all else being equal, core formation at lower temperatures should promote greater isotope fractionation. If temperatures of core–mantle equilibration over time reflect that of the peridotite liquidus at the interface, then temperature should be directly proportional to pressure (given the positive dP/dT slope of the peridotite liquidus; Fiquet et al., 2010). Manganese becomes more siderophile at higher temperatures, with little effect of pressure (Mann et al., 2009). As a result, smaller bodies might be expected to show higher isotope fractionation and lower Fe/Mn ratios. However, the Eucrite parent body (IV-Vesta), despite undergoing core formation at relatively low temperature (≈1900 K, Righter and Drake, 1996), records no departure in iron isotope composition from that of chondrites. By contrast, the Earth, whose core last equilibrated with the mantle at 2500–3500 K (Wood et al., 2006), does exhibit resolvable fractionation. Furthermore, liquid metal and liquid silicate are isotopically indistinguishable in experiments between

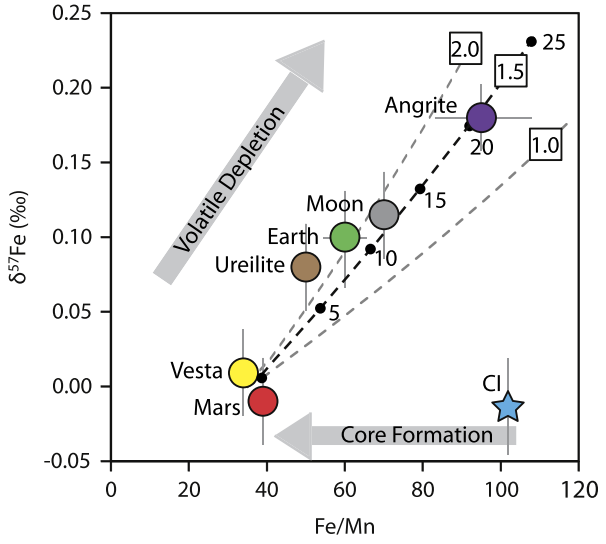

Fig. 7. A compilation of iron isotope compositions of planetary basalts (see Section 5.1 for data sources) as a function of their Fe/Mn ratio, taken from O'Neill and Palme (2008). Core formation causes a net decrease in Fe/Mn with minimal isotope fractionation, whereas volatile depletion enriches the residuum in both Fe/Mn and δ^{57}Fe. Dashed lines indicate evolving Fe/Mn and δ^{57}Fe as a result of volatile depletion at 1300 K, with isotope fractionation factors between $FeO_{(l,s)}$ and $Fe_{(g)}$ varying from 2, 1.5 and $1 \times 10^6/T^2$. Numbers represent the percentage of iron loss. Note that the arrows do not necessarily represent the order; i.e., volatile depletion may have occurred first (Section 5.3).

1–7.7 GPa and 1250–2000 °C (Hin et al., 2012; Poitrasson et al., 2009) or light isotope enrichment in the silicate in the presence of S occurs (Shahar et al., 2015), opposite to that observed. Despite this, Barrat et al. (2015) appeal to S-rich metal segregation to explain the heavy composition of ureilites. Nonetheless, Mars' core is estimated to have ~15 wt% S (Dreibus and Wanke, 1985), yet its composition is chondritic. The vector of isotope fractionation changes at high pressures, however owing to the incorporation of Fe^{3+} in bridgmanite (Williams et al., 2012), a condition relevant to the Earth. However, mass balance dictates that this mechanism is not sufficient to generate a significant fractionation (Craddock et al., 2013) and in any case would not apply to the much smaller angrite parent body which nevertheless has the most ^{57}Fe-enriched basalts. Additionally, since Mn does not appreciably partition into the core ($\log K_D = -1.5$ to -3) except under very high temperatures (Mann et al., 2009), core formation would impart a relatively uniform Fe/Mn ratio in planetary mantles, lower than chondrites (Fig. 7). The Earth could be an exception to this, since its core formed at higher temperatures, thereby potentially further depleting Mn relative to other planetary bodies. However, the non-systematic relationship between iron isotope fractionation and modes of core formation, compounded by the lack of fractionation observed experimentally, render core formation an unlikely mechanism of generating the heavy isotope compositions of planetary basalts.

5.3. Volatile depletion

The temperature at which 1/2 of the Mn budget of the nebular gas is condensed, 1158 K, is almost 200 K lower than that of Fe (1334 K, Lodders, 2003). Hence, incomplete condensation or evaporation should increase the Fe/Mn ratio of the solid, processes thought to create Fe/Mn variations in planetary basalts (Drake et al., 1989; Papike et al., 2003). From the hierarchy in Fig. 7, angrites have experienced the greatest volatile depletion, followed by the Moon, Earth, ureilites then Mars and Vesta. These systematics are compatible with a scenario in which volatile depletion (manifest as an increase in Fe/Mn) is associated with heavy isotope enrichment in the residue. Volatile loss during a giant impact has been proposed to account for the anomalously heavy Earth–Moon system (Poitrasson et al., 2004). However, identification of other bodies with similar (ureilites) or more extreme (angrites) signatures suggests this may be a common process in the inner solar system.

The extent of volatile depletion of an element, E, in a body (B) can be quantified by normalising it to a lithophile element thought not to be volatile, in this case, Mg. This ratio is then normalised to CI chondrites, whose abundances of moderately volatile elements match that of the solar photosphere, to give the elemental depletion factor, f_E:

$$f_E = \frac{(E/\mathrm{Mg})_B}{(E/\mathrm{Mg})_{CI}}. \tag{3}$$

In Mars and IV-Vesta $f_{Mn} \approx 1$, implying no loss of Mn during their accretion. Since $T_c^{Fe} > T_c^{Mn}$, iron loss from these bodies did not occur, and, accordingly they preserve chondritic δ^{57}Fe ratios. Depletion factors for Mn in the Moon, Earth and angrites are comparable, 0.2–0.3, and are also associated with the heaviest δ^{57}Fe values, suggestive of a causative link between the two parameters. How, mechanistically, such a correlation might arise depends on the timing and locus of volatile depletion. Both Mn/Na (O'Neill and Palme, 2008) and Mn–Cr isotope systematics (Moynier et al., 2007) suggest Mn depletion in the Earth is nebular, that is, it occurred contemporaneously with that observed in chondritic meteorites. This, however, poses a problem since chondritic meteorites have uniform iron isotope compositions (Craddock and Dauphas, 2011), despite depletions in Mn. In carbonaceous chondrites (the only class 3 chondrites to show Mn depletion), f_{Mn} only extends to ≈0.5, and iron loss is minimal (Wasson and Kallemeyn, 1988), with resulting Fe/Mn ratios varying to an extent similar to that in planetary basalts. Therefore, the isotopic homogeneity among chondritic meteorites may be due to less extreme volatile depletion at lower temperatures (causing Mn loss but not appreciable Fe) compared with Earth's precursors. Conversely, the superchondritic Mn/Na of angrites suggests that they underwent volatile loss at significantly higher oxygen fugacities (O'Neill and Palme, 2008), that is, after dissipation of the solar nebula. Nevertheless, multiple volatile depletion events cannot be excluded, for example, a nebular depletion that affected Fe and Mn, followed by a post-nebular process that resulted in Na loss. Regardless, extensive volatile depletion in angrites with respect to the Earth, as recorded by K/U or Na/Ti ratios (O'Neill and Palme, 2008), is consistent with their heavy Fe isotope composition.

Iron and manganese share another useful property; the stable gaseous species of both take the form of monatomic metals ($Mn_{(g)}$ and $Fe_{(g)}$; Fegley, 1993), such that their dependence on the redox state of the gas is comparable. As much is observed in heating experiments, where Fe and Mn evaporate together (Floss et al., 1997). Writing expressions for their volatilisation,

$$FeO_{(l,s)} = Fe_{(g)} + \frac{1}{2}O_2, \tag{4}$$

$$MnO_{(l,s)} = Mn_{(g)} + \frac{1}{2}O_2, \tag{5}$$

demonstrates that the effect of oxygen fugacity cancels such that the two reactions can be equated, yielding:

$$MnO_{(l,s)} + Fe_{(g)} = FeO_{(l,s)} + Mn_{(g)}. \tag{6}$$

and, at equilibrium, leads to

$$\ln K = \ln\left(\frac{a\mathrm{FeO}_{(l,s)}}{p\mathrm{Fe}_{(g)}} \times \frac{p\mathrm{Mn}_{(g)}}{a\mathrm{MnO}_{(l,s)}}\right) = \frac{-(\Delta G^o_{\mathrm{Mn-MnO}} - \Delta G^o_{\mathrm{Fe-FeO}})}{RT}. \tag{7}$$

Here, ΔG^o are the standard state free energies for the reactions of the metal–oxide pair, R the gas constant and T the temperature in Kelvin (note that ideality is assumed). For a finite elemental budget, $M_{(g)}$ is the proportion of the metal in the gas, and therefore $MO_{(l,s)} = (1 - M_{(g)})$. Employing existing thermodynamic data (Chase, 1998), $\Delta G^o_{\text{Fe–Mn}}$ (kJ/mol) $= -51.7 + 0.0908T - 0.00977T\ln(T)$, such that the relative fraction of Fe to Mn in the gas, assuming a constant pressure, is dependent only on temperature. If volatile depletion occurred at high temperatures (e.g. 3000 K during a giant impact; Melosh, 1990), a similar fraction of Fe and Mn would be lost, implying wholesale iron depletion in terrestrial bodies, which is not recorded. Therefore, volatile depletion must have taken place at significantly lower temperatures, ≈1300 K, as constrained by element abundances in the Earth and Moon for a giant impact scenario (O'Neill, 1991), or upon equilibrium condensation of the solar nebula. Since Fe depletion relative to Mn is independent of f_{O_2}, these two scenarios cannot be distinguished on the basis of Fe/Mn ratios alone, though Mn (and therefore Fe) depletion in the Earth appears to be nebular in origin, as discussed above. Conversely, the Moon's slightly higher Fe/Mn ratio (≈70) relative to the Earth permits additional, post-nebular volatile loss, perhaps during the giant impact, though again at 1300 K (O'Neill, 1991). Therefore, adopting temperatures of 1300 K, and an initial Fe/Mn of 35 (Fig. 7), the Fe/Mn ratio in the residual solid as a function of volatile depletion is modelled. Under these conditions, 7 ± 2% Fe depletion is required to explain the Fe/Mn ratio of the silicate Earth (60 ± 6), 10 ± 1% for the Moon, and 20 ± 5% for angrites (Fe/Mn = 95 ± 13).

Whether such a process can reproduce the isotopic trend observed in Fig. 7 requires prior knowledge of FeO–Fe$_{(g)}$ isotope fractionation factors, which are, unfortunately, lacking. However, fractionation factors for the equivalent reaction between MgO in olivine and Mg$_{(g)}$ have been determined, where $\Delta^{26}Mg_{MgO-Mg} = 2.2 \times 10^6/T^2$‰ (Schauble, 2011). Given the ideality of the Fe–Mg solid solution in olivine (Bradley, 1962) and the equality in volatilisation reaction stoichiometry (eq. (4)) for Fe and Mg, to a good approximation, the iron isotope fractionation factor can be simply related to that of Mg by the relative isotopic mass difference:

$$\Delta^{57}Fe_{FeO-Fe} = \frac{(\frac{57-54}{57})}{(\frac{26-24}{26})} \times \Delta^{26}Mg_{MgO-Mg} = 1.5 \times 10^6/T^2‰. \quad (8)$$

At 1300 K, $\Delta^{57}Fe_{FeO-Fe} = 0.9$‰. The isotopic composition of the solid or liquid (FeO) is found assuming a closed-system, Rayleigh distillation process, wherein:

$$\delta^{57}Fe_{FeO} = \delta^{57}Fe_{Bulk} + \Delta^{57}Fe_{FeO-Fe}\ln(f_{FeO}). \quad (9)$$

$\delta^{57}Fe_{Bulk}$ is assumed to be chondritic (0‰ for simplicity), and f_{FeO} is given by eq. (7). Together, these calculations very faithfully match the observed iron isotope trends in planetary basalts (Fig. 7). Upon solar nebula condensation, Fe also partitions into metal, particularly in enstatite chondrites. However, since FeO (in olivine or silicate liquid) has an indistinguishable isotope composition to Fe metal at 1523 K (e.g., Hin et al., 2012) and in unequilibrated chondrites (Theis et al., 2008), the net isotope fractionation factor (eq. (8)) will be little affected.

5.4. A volatile history of the terrestrial planets

That Fe is controlled by volatility-related processes is also substantiated by Si isotopes (Fig. 8). Despite their vastly different geochemical properties, iron and silicon isotopes in planetary basalts are remarkably well correlated (Fig. 8), suggesting that planetary isotope differences are faithfully captured by basaltic rocks.

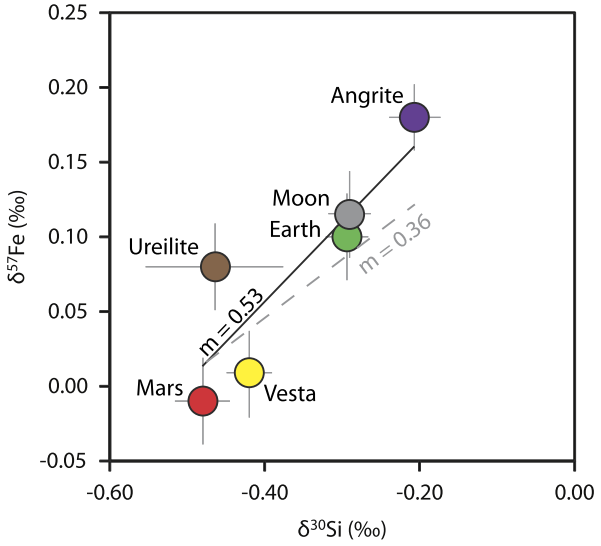

Fig. 8. The relationship between iron and silicon isotopes (compiled from Dauphas et al., 2015) in planetary basalts. The best fit slope is = 0.53, whereas that predicted by isotopic fractionation between olivine and gas for both Fe and Si gives the theoretical slope of 0.36.

The large Si isotope metal–silicate fractionation (Hin et al., 2014; Shahar et al., 2011), is, alone, insufficient in explaining the isotopic discrepancy between chondrites and Earth (Zambardi et al., 2013), and especially angrites, whose parent body would have no Si in its core (Dauphas et al., 2015; Pringle et al., 2014). Furthermore, iron- and silicon isotope metal–silicate fractionation factors are in opposing directions (compare Hin et al., 2014 and Shahar et al., 2015), and therefore a negative correlation would be expected if core formation was the controlling influence. Rather, to explain Si isotope variations, volatile processes have been widely championed, either at a late (Pringle et al., 2014; Zambardi et al., 2013) or early, nebular stage (Dauphas et al., 2015). Silicon, like Fe, is not normally volatile during nebular condensation (e.g. Wasson and Kallemeyn, 1988) or evaporation, except, it appears, in cases where volatile depletion is pronounced, as for the Earth–Moon system and angrite parent body. The fractionation factor between SiO_2 (in forsterite) and $SiO_{(g)}$, the stable gas phase, is $\Delta^{30}Si = 4.2 \times 10^6/T^2$ (Dauphas et al., 2015), ∼3× larger than that for $\Delta^{57}Fe$ (Eq. (8)), predicting a slope of 0.36 in Fig. 8. The observed slope, ∼0.5, indicates larger Fe isotope variation than expected, which could arise from the slightly higher volatility of Fe than Si. Isotopic characterisation of inner solar system bodies for elements that bracket the volatility of Fe, but otherwise behave similarly during igneous processes, namely Zn and Mg, may aid in further elucidating causes of isotope fractionation.

Mars and IV-Vesta preserve their initial Mn budget and are unfractionated from chondritic meteorites in Fe–Si isotope space. In the case of the Earth, volatile depletion is probably nebular, implying that the composition of the Earth is non-chondritic, with respect to both Si and Fe. That the Moon shows a composition indistinguishable (Si) or close to (Fe) that of the Earth lends support to the idea that it was inherited from the Earth's mantle, as suggested by elemental abundances and isotope systematics (O'Neill, 1991; Ringwood and Kesson, 1977; Zhang et al., 2012). However, the slight differences in Fe/Mn and potentially Fe isotopes (Wang et al., 2015) between the Earth and Moon allow for further lunar volatile depletion, perhaps attending the giant impact. Angrites exhibit the most extreme fractionation in all indices; Fe/Mn, $\delta^{30}Si$ and $\delta^{57}Fe$. Although their non-chondritic Mn/Na suggests post-nebular volatile depletion, Rb–Sr chronology permits the possibility of incomplete nebular condensation, too (Hans et al., 2013). All plane-

tary basalts show differing patterns of moderately-volatile element depletion relative to carbonaceous chondrites. These patterns are the sum of physicochemical parameters such as temperature and oxygen fugacity, and dynamical controls including impact energetics and frequency, and solid–gas mechanics. Therefore, much of the interpretation of the evolution of the terrestrial planets hinges upon the style and timing of volatile depletion, the details of which remain uncertain.

6. Conclusion

Application of the olivine–melt equilibrium Fe–Mg K_D reveals that few Martian shergottites are representative of liquid compositions, with several more falling on olivine control lines that allow for correction to primary magmas. These have Mg#s between 0.5 and 0.65, which can be modelled, using *alphaMELTS*, to be 10–50% partial melts of a Martian mantle with Mg# = 0.77. The iron isotope compositions of SNC meteorites become heavier for more evolved magmas, defining an array with $\Delta^{57}Fe_{Min\text{-}Melt} = -0.1‰$, smaller than that for terrestrial magmas. This reflects the more reduced redox state of Fe in Martian magmas, resulting in lower $\Delta^{57}Fe_{Min\text{-}Melt}$. At the same Mg#, Martian basalts are ≈0.1‰ lighter than terrestrial tholeiitic basalts. Extrapolation of the correlation between δ^{57}Fe and Mg# for SNCs yields a Martian mantle value of $-0.04 \pm 0.03‰$ (1SD), appreciably lighter than that of Earth at the 1SD level, but within uncertainty of chondrites. Owing to the paucity of mantle samples from other planetary bodies, primitive basalts rocks are used to investigate causes of iron isotope fractionation during planetary accretion. Basaltic rocks vary from chondritic values (δ^{57}Fe ≈0‰) in Mars and IV-Vesta, +0.1‰ in the Earth and Moon and up to +0.2‰ in angrites, as a positive function of their Fe/Mn ratio and Si isotope composition. Such variation can be explained by progressive volatile depletion giving rise to heavy values in the residuum. For the Earth, iron isotope fractionation likely arises during solar nebula condensation, near 1300 K, requiring ∼7% Fe depletion, however additional, post-nebular volatile loss might have occurred on the Moon and the angrite parent body.

Acknowledgements

Discussions with Hugh O'Neill on the thermodynamic and geochemical behaviour of the elements during planetary formation and differentiation helped to clarify a number of the concepts treated in this study; P.A.S's intellectual debt to Hugh should be obvious. Many thanks to Ghylaine Quitté, Alex Halliday and Marc Hirschmann for helpful suggestions on earlier versions of the work. We greatly appreciate the comments of two anonymous reviewers, one in particular that urged us to think critically regarding planetary differences and diffusive processes. The even-handed and efficient editorial input of Bernard Marty is gratefully acknowledged. We graciously thank K. Righter of NASA for providing the MWG samples. This work was partially supported by an Australian Postgraduate Award and ANU Vice Chancellor's Scholarship to P.A.S., the Australian Research Council by a DECRA fellowship to O.N. (DE120100513) and the UK Science and Technology Facilities Council (STFC) grants to M.A. (grant nos. ST/I001298/1 & ST/L000776/1). Analytical work in Toulouse was supported by a CNRS-INSU PNP grant to F.P.

Appendix A. Supplementary material

Supplementary material related to this article can be found online at http://dx.doi.org/10.1016/j.epsl.2016.05.030.

References

Anand, M., Russell, S.S., Blackhurst, R.L., Grady, M.M., 2006. Searching for signatures of life on Mars: an Fe-isotope perspective. Philos. Trans. R. Soc. Lond. B, Biol. Sci. 361, 1715–1720.

Arndt, N.T., 1976. Melting relations of ultramafic lavas (komatiites) at 1 atm and high pressure. Year B. - Carnegie Inst. Wash. 75, 555–562.

Barrat, J.A., Blichert-Toft, J., Gillet, P., Keller, F., 2000. The differentiation of eucrites: the role of in situ crystallization. Meteoritics 35, 1087–1100.

Barrat, J.A., Rouxel, O., Wang, K., Moynier, F., Yamaguchi, A., Bischoff, A., Langlade, J., 2015. Early stages of core segregation recorded by Fe isotopes in an asteroidal mantle. Earth Planet. Sci. Lett. 419, 93–100.

Basu Sarbadhikari, A., Day, J.M.D., Liu, Y., Rumble, D., Taylor, L.A., 2009. Petrogenesis of olivine-phyric shergottite Larkman Nunatak 06319: implications for enriched components in martian basalts. Geochim. Cosmochim. Acta 73, 2190–2214.

Beard, B.L., Johnson, C.M., 2004. Inter-mineral Fe isotope variations in mantle-derived rocks and implications for the Fe geochemical cycle. Geochim. Cosmochim. Acta 68, 4727–4743.

Bédard, J.H., 2010. Parameterization of the Fe–Mg exchange coefficient (K_D) between clinopyroxene and silicate melts. Chem. Geol. 274, 169–176.

Bézos, A., Humler, E., 2005. The $Fe^{3+}/\Sigma Fe$ ratios of MORB glasses and their implications for mantle melting. Geochim. Cosmochim. Acta 69 (3), 711–725.

Blichert-Toft, J., Gleason, J.D., Telouk, P., Albarède, F., 1999. The Lu–Hf isotope geochemistry of shergottites and the evolution of the Martian mantle–crust system. Earth Planet. Sci. Lett. 173, 25–39.

Borg, L.E., Draper, D.S., 2003. A petrogenetic model for the origin and compositional variation of the martian basaltic meteorites. Meteorit. Planet. Sci. 38, 1713–1731.

Bradley, R.S., 1962. Thermodynamic calculations on phase equilibria involving fused salts, part 2: solid solutions and application to the olivines. Am. J. Sci. 260, 550–554.

Bridges, J.C., Warren, P.H., 2006. The SNC meteorites: basaltic igneous processes on Mars. J. Geol. Soc. 163, 229–251.

Chase, M.W., 1998. NIST-JANAF Thermochemical Tables, 4th edition. American Chemical Society, Washington, DC.

Chen, L.M., Song, X.Y., Zhu, X.K., Zhang, X.Q., Yu, S.Y., Yi, J.N., 2014. Iron isotope fractionation during crystallization and sub-solidus re-equilibration: constraints from the Baima mafic layered intrusion, SW China. Chem. Geol. 380, 97–109.

Craddock, P.R., Dauphas, N., 2011. Iron isotopic compositions of geological reference materials and chondrites. Geostand. Geoanal. Res. 35, 101–123.

Craddock, P.R., Warren, J.M., Dauphas, N., 2013. Abyssal peridotites reveal the near-chondritic Fe isotopic composition of the Earth. Earth Planet. Sci. Lett. 365, 63–76.

Dauphas, N., Craddock, P.R., Asimow, P.D., Bennett, V.C., Nutman, A.P., Ohnenstetter, D., 2009. Iron isotopes may reveal the redox conditions of mantle melting from Archean to Present. Earth Planet. Sci. Lett. 288, 255–267.

Dauphas, N., Roskosz, M., Alp, E.E., Neuville, D.R., Hu, M.Y., Sio, C.K., Tissot, F.L.H., Zhao, J., Tissandier, L., Médard, E., Cordier, C., 2014. Magma redox and structural controls on iron isotope variations in Earth's mantle and crust. Earth Planet. Sci. Lett. 398, 127–140.

Dauphas, N., Poitrasson, F., Burkhardt, C., Kobayashi, H., 2015. Planetary and meteoritic Mg/Si and δ^{30}Si variations inherited from solar nebula chemistry. Earth Planet. Sci. Lett. 427, 236–248.

Davis, F.A., Humayun, M., Hirschmann, M.M., Cooper, R.S., 2013. Experimentally determined mineral/melt partitioning of first-row transition elements (FRTE) during partial melting of peridotite at 3 GPa. Geochim. Cosmochim. Acta 104, 232–260.

Day, J.M.D., Taylor, L.A., Floss, C., Mcsween, H.Y., 2006. Petrology and chemistry of MIL 03346 and its significance in understanding the petrogenesis of nakhlites on Mars. Meteorit. Planet. Sci. 41, 581–606.

Drake, M.J., Newsom, H.E., Capobianco, C.J., 1989. V, Cr, and Mn in the Earth, Moon, EPB, and SPB and the origin of the Moon: experimental studies. Geochim. Cosmochim. Acta 53, 2101–2111.

Dreibus, G., Wanke, H., 1985. Mars, a volatile-rich planet. Meteoritics 20, 367–381.

Elkins-Tanton, L.T., Parmentier, E.M., Hess, P.C., 2003. Magma ocean fractional crystallization and cumulate overturn in terrestrial planets: implications for Mars. Meteorit. Planet. Sci. 38, 1753–1771.

Elkins-Tanton, L.T., Hess, P.C., Parmentier, E.M., 2005. Possible formation of ancient crust on Mars through magma ocean processes. J. Geophys. Res. 110, 1–11.

Fegley, B., 1993. Chemistry of the Solar Nebula. In: Greenberg, J.M., et al. (Eds.), The Chemistry of Life's Origins. Kluwer Academic Publishers, Amsterdam, pp. 75–147.

Filiberto, J., Dasgupta, R., 2011. Fe^{2+}–Mg partitioning between olivine and basaltic melts – applications to genesis of olivine-phyric shergottites and conditions of melting in the Martian interior. Earth Planet. Sci. Lett. 304, 527–537.

Fiquet, G., Auzende, A.L., Siebert, J., Corgne, A., Bureau, H., Ozawa, H., Garbarino, G., 2010. Melting of peridotite to 140 gigapascals. Science 329, 1516–1518. http://dx.doi.org/10.1126/science.1192448.

Floss, C., Goresy, A.E.L., Zinner, E., Kransel, G., Rammensee, W., Palme, H., 1997. Elemental and isotopic fractionations produced through evaporation of the Al-

lende CV chondrite: implications for the origin of HAL-type hibonite inclusions. Geochim. Cosmochim. Acta 60, 1975–1997.
Goodrich, C.A., 2003. Petrogenesis of olivine-phyric shergottites Sayh al Uhaymir 005 and Elephant Moraine A79001 lithology A. Geochim. Cosmochim. Acta 67, 3735–3772.
Green, D.H., Ringwood, A.E., Hibberson, W.O., Ware, N.G., 1975. Experimental petrology of Apollo 17 mare basalts. In: 6th Proc. Lunar Planet. Sci. Conf., pp. 871–893.
Halliday, A.N., Wanke, H., Birck, J.-L., Clayton, R.N., 2001. The accretion, composition and early differentiation of Mars. Space Sci. Rev. 96, 197–230.
Hans, U., Kleine, T., Bourdon, B., 2013. Rb–Sr chronology of volatile depletion in differentiated protoplanets: BABI, ADOR and ALL revisited. Earth Planet. Sci. Lett. 374, 204–214.
Herd, C.D.K., 2003. The oxygen fugacity of olivine-phyric martian basalts and the components within the mantle and crust of Mars. Meteorit. Planet. Sci. 38, 1793–1805.
Herd, C.D.K., Borg, L.E., Jones, J.H., Papike, J.J., 2002. Oxygen fugacity and geochemical variations in the martian basalts: implications for martian basalt petrogenesis and the oxidation state of the upper mantle of Mars. Geochim. Cosmochim. Acta 66, 2025–2036.
Hin, R.C., Fitoussi, C., Schmidt, M.W., Bourdon, B., 2014. Experimental determination of the Si isotope fractionation factor between liquid metal and liquid silicate. Earth Planet. Sci. Lett. 387, 55–66.
Hin, R.C., Schmidt, M.W., Bourdon, B., 2012. Experimental evidence for the absence of iron isotope fractionation between metal and silicate liquids at 1 GPa and 1250–1300 °C and its cosmochemical consequences. Geochim. Cosmochim. Acta 93, 164–181.
Jarosewich, E., 1990. Chemical analyses of meteorites: a compilation of stony and iron meteorite analyses. Meteoritics 25 (4), 323–337.
Jenner, F.E., O'Neill, H.S.C., 2012. Analysis of 60 elements in 616 ocean floor basaltic glasses. Geochem. Geophys. Geosyst. 13, Q02005. http://dx.doi.org/10.1029/2011GC004009.
Jones, J.H., 1989. Isotopic relationships among the shergottites, the nakhlites and Chassigny. In: Proceedings of the 19th Lunar and Planetary Science Conference, pp. 465–474.
Khan, A., Connolly, J.A.D., 2008. Constraining the composition and thermal state of Mars from inversion of geophysical data. J. Geophys. Res. 113, E07003.
Liu, Y., Spicuzza, M.J., Craddock, P.R., Day, J.M.D., Valley, J.W., Dauphas, N., Taylor, L.A., 2010. Oxygen and iron isotope constraints on near-surface fractionation effects and the composition of lunar mare basalt source regions. Geochim. Cosmochim. Acta 74, 6249–6262.
Liu, Y., Balta, J.B., Goodrich, C.A., McSween, H.Y., Taylor, L.A., 2013. New constraints on the formation of shergottite Elephant Moraine 79001 lithology A. Geochim. Cosmochim. Acta 108, 1–20.
Lodders, K., 2003. Solar system abundances and condensation temperatures of the elements. Astrophys. J. 591, 1220–1247.
Mann, U., Frost, D.J., Rubie, D.C., 2009. Evidence for high-pressure core–mantle differentiation from the metal–silicate partitioning of lithophile and weakly-siderophile elements. Geochim. Cosmochim. Acta 73, 7360–7386.
Melosh, H.J., 1990. Giant impacts and the thermal state of the early Earth. In: Newsom, H.E., Jones, J.H. (Eds.), Origin of the Earth. Oxford University, New York, pp. 69–83.
Moynier, F., Yin, Q., Jacobsen, B., 2007. Dating the first stage of planet formation. Astrophys. J. 671, 181–183.
Musselwhite, D.S., Dalton, H.A., Kiefer, W.S., Treiman, A.H., 2006. Experimental petrology of the basaltic shergottite Yamato-980459: implications for the thermal structure of the Martian mantle. Meteorit. Planet. Sci. 41, 1271–1290.
Needham, A.W., Porcelli, D., Russell, S.S., 2009. An Fe isotope study of ordinary chondrites. Geochim. Cosmochim. Acta 73, 7399–7413.
Oeser, M., Dohmen, R., Horn, I., Schuth, S., Weyer, S., 2015. Processes and time scales of magmatic evolution as revealed by Fe–Mg chemical and isotopic zoning in natural olivines. Geochim. Cosmochim. Acta 154, 130–150.
O'Neill, H.S.C., 1991. The origin of the Moon and the early history of the Earth – a chemical model, part 1: the Moon. Geochim. Cosmochim. Acta 55, 1135–1157.
O'Neill, H.S.C., Canil, D., Rubie, D.C., 1998. Oxide–metal equilibria to 2500 C and 25 GPa: implications for core formation and the light component in the Earth's core. J. Geophys. Res. 103, 12239–12260.
O'Neill, H.S.C., Palme, H., 2008. Collisional erosion and the non-chondritic composition of the terrestrial planets. Philos. Trans. R. Soc., Math. Phys. Eng. Sci. 366, 4205–4238.
Palme, H., O'Neill, H.S.C., 2014. Cosmochemical estimates of mantle composition. In: Carlson, R.W. (Ed.), Treatise on Geochemistry, Vol. 3: The Mantle and Core. Elsevier B.V., Amsterdam, pp. 1–39.
Papike, J.J., Karner, J.M., Shearer, C.K., 2003. Determination of planetary basalt parentage: a simple technique using the electron microprobe. Am. Mineral. 88, 469–472.
Poitrasson, F., 2007. Does planetary differentiation really fractionate iron isotopes? Earth Planet. Sci. Lett. 256, 484–492.
Poitrasson, F., Freydier, R., 2005. Heavy iron isotope composition of granites determined by high resolution MC-ICP-MS. Chem. Geol. 222, 132–147.
Poitrasson, F., Halliday, A.N., Lee, D.-C., Levasseur, S., Teutsch, N., 2004. Iron isotope differences between Earth, Moon, Mars and Vesta as possible records of contrasted accretion mechanisms. Earth Planet. Sci. Lett. 223, 253–266.
Poitrasson, F., Roskosz, M., Corgne, A., 2009. No iron isotope fractionation between molten alloys and silicate melt to 2000 °C and 7.7 GPa: experimental evidence and implications for planetary differentiation and accretion. Earth Planet. Sci. Lett. 278, 376–385.
Poitrasson, F., Delpech, G., Grégoire, M., 2013. On the iron isotope heterogeneity of lithospheric mantle xenoliths: implications for mantle metasomatism, the origin of basalts and the iron isotope composition of the Earth. Contrib. Mineral. Petrol. 165, 1243–1258.
Polyakov, V.B., 2009. Equilibrium iron isotope fractionation at core–mantle boundary conditions. Science 323 (5916), 912–914.
Polyakov, V.B., Mineev, S.D., 2000. The use of Mössbauer spectroscopy in stable isotope geochemistry. Geochim. Cosmochim. Acta 64, 849–865.
Pringle, E.A., Moynier, F., Savage, P.S., Badro, J., Barrat, J., 2014. Silicon isotopes in angrites and volatile loss in planetesimals. Proc. Natl. Acad. Sci. USA 111, 17029–17032.
Prinz, M., Hlava, P.H., Keil, K., 1974. The Chassigny meteorite: a relatively iron-rich cumulate dunite. Meteoritics 9, 393–394.
Qin, L., Humayun, M., 2008. The Fe/Mn ratio in MORB and OIB determined by ICP-MS 72. Geochim. Cosmochim. Acta 72, 1660–1677.
Rai, N., van Westrenen, W., 2013. Core–mantle differentiation in Mars. J. Geophys. Res., Planets 118, 1195–1203.
Richter, F., Chaussidon, M., Mendybaev, R., Kite, E., 2016. Reassessing the cooling rate and geologic setting of Martian meteorites MIL 03346 and NWA 817. Geochim. Cosmochim. Acta 182, 1–23.
Righter, K., Drake, M.J., 1996. Core formation in Earth's Moon, Mars, and Vesta. Icarus 124, 513–529.
Righter, K., Danielson, L.R., Pando, K., Morris, R.V., Graff, T.G., Agresti, D.G., Martin, A.M., Sutton, S.R., Newville, M., Lanzirotti, A., 2013. Redox systematics of martian magmas with implications for magnetite stability. Am. Mineral. 98, 616–628.
Ringwood, A.E., Hibberson, W., 1991. Solubilities of mantle oxides in molten iron at high pressures and temperatures: implications for the composition and formation of Earth's core. Earth Planet. Sci. Lett. 102, 235–251. http://dx.doi.org/10.1016/0012-821X(91)90020-I.
Ringwood, A.E., Kesson, S.E., 1977. Basaltic magmatism and the bulk composition of the moon. Moon 16, 425–464. http://dx.doi.org/10.1007/BF00577902.
Roeder, P.L., Emslie, R.F., 1970. Olivine–liquid equilibrium. Contrib. Mineral. Petrol. 29, 275–289.
Roskosz, M., Luais, B., Watson, H., Toplis, M., Alexander, C., Mysen, B., 2006. Experimental quantification of the fractionation of Fe isotopes during metal segregation from a silicate melt. Earth Planet. Sci. Lett. 248, 851–867. http://dx.doi.org/10.1016/j.epsl.2006.06.037.
Rubie, D.C., Jacobson, S.A., 2015. Mechanisms and geochemical models of core formation. In: Fischer, R., Terasaki, H. (Eds.), Deep Earth: Physics and Chemistry of the Lower Mantle and Core. Chicago, pp. 1–20.
Schauble, E.A., 2004. Applying stable isotope fractionation theory to new systems. In: Johnson, C.M., Beard, B.L., Albaréde, F. (Eds.), Reviews in Mineralogy and Geochemistry: Geochemistry of Non-Traditional Stable Isotopes. Mineralogical Society of America, Washington DC, pp. 65–111.
Schauble, E.A., 2011. First-principles estimates of equilibrium magnesium isotope fractionation in silicate, oxide, carbonate and hexaaquamagnesium(2+) crystals. Geochim. Cosmochim. Acta 75, 844–869.
Schoenberg, R., von Blanckenburg, F., 2006. Modes of planetary-scale Fe isotope fractionation. Earth Planet. Sci. Lett. 252, 342–359.
Shahar, A., Young, E.D., Manning, C.E., 2008. Equilibrium high-temperature Fe isotope fractionation between fayalite and magnetite: an experimental calibration. Earth Planet. Sci. Lett. 268, 330–338.
Shahar, A., Hillgren, V.J., Young, E.D., Fei, Y., Macris, C.A., Deng, L., 2011. High-temperature Si isotope fractionation between iron metal and silicate. Geochim. Cosmochim. Acta 75, 7688–7697. http://dx.doi.org/10.1016/j.gca.2011.09.038.
Shahar, A., Hillgren, V.J., Horan, M.F., Mesa-Garcia, J., Kaufman, L.A., Mock, T.D., 2015. Sulfur-controlled iron isotope fractionation experiments of core formation in planetary bodies. Geochim. Cosmochim. Acta 150, 253–264.
Shearer, C.K., Burger, P.V., Papike, J.J., Borg, L.E., Irving, A.J., Herd, C., 2008. Petrogenetic linkages among Martian basalts: implications based on trace element chemistry of olivine. Meteorit. Planet. Sci. 43, 1241–1258.
Shearer, C.K., Aaron, P.M., Burger, P.V., Guan, Y., Bell, A.S., Papike, J.J., Sutton, S.R., 2013. Petrogenetic linkages among fO_2, isotopic enrichments-depletions and crystallization history in martian basalts: evidence from the distribution of phosphorus and vanadium valence state in olivine megacrysts. In: 44th Lunar and Planetary Science Conference, pp. 2326–2327.
Sio, C.K.I., Dauphas, N., Teng, F., Chaussidon, M., Helz, R.T., Roskosz, M., 2013. Discerning crystal growth from diffusion profiles in zoned olivine by in situ Mg–Fe isotopic analyses. Geochim. Cosmochim. Acta 123, 302–321.
Sio, C.K., Chaussidon, M., Dauphas, N., Richter, F.M., Roskosz, M., Sautter, V., 2014. Determining the nature of olivine zoning in nakhlites by in-situ Mg and Fe iso-

topic analyses. In: 45th Lunar and Planetary Science Conference.
Smith, P.M., Asimow, P.D., 2005. Adiabat_1ph: a new public front-end to the MELTS, pMELTS, and pHMELTS models. Geochem. Geophys. Geosyst. 6, Q02004. http://dx.doi.org/10.1029/2004GC000816.
Sossi, P.A., Foden, J.D., Halverson, G.P., 2012. Redox-controlled iron isotope fractionation during magmatic differentiation: an example from the Red Hill intrusion, S. Tasmania. Contrib. Mineral. Petrol. 164, 757–772.
Sossi, P.A., Halverson, G.P., Nebel, O., Eggins, S.M., 2015. Combined separation of Cu, Fe and Zn from rock matrices and improved analytical protocols for stable isotope determination. Geostand. Geoanal. Res. 39 (2), 129–149.
Taylor, G.J., 2013. The bulk composition of Mars. Chem. Erde 73, 401–420.
Teng, F.-Z., Dauphas, N., Helz, R.T., 2008. Iron isotope fractionation during magmatic differentiation in Kilauea Iki lava lake. Science 320, 1620–1622.
Teng, F.-Z., Dauphas, N., Huang, S., Marty, B., 2013. Iron isotopic systematics of oceanic basalts. Geochim. Cosmochim. Acta 107, 12–26.
Theis, K.J., Burgess, R., Lyon, I.C., Sears, D.W., 2008. The origin and history of ordinary chondrites: a study by iron isotope measurements of metal grains from ordinary chondrites. Geochim. Cosmochim. Acta 72, 4440–4456.
Toplis, M.J., 2005. The thermodynamics of iron and magnesium partitioning between olivine and liquid: criteria for assessing and predicting equilibrium in natural and experimental systems. Contrib. Mineral. Petrol. 149, 22–39.
Usui, T., McSween, H.Y., Floss, C., 2008. Petrogenesis of olivine-phyric shergottite Yamato 980459, revisited. Geochim. Cosmochim. Acta 72 (6), 1711–1730.
von Seckendorff, V., O'Neill, H.S.C., 1993. An experimental study of Fe–Mg partitioning between olivine and orthopyroxene at 1173, 1273 and 1423 K and 1.6 GPa. Contrib. Mineral. Petrol. 113, 196–207.
Wadhwa, M., 2001. Redox state of Mars' upper mantle and crust from Eu anomalies in shergottite pyroxenes. Science 291, 1527–1530.
Wadhwa, M., 2008. Redox conditions on small bodies, the Moon and Mars. Rev. Mineral. Geochem. 68, 493–510.
Wadhwa, M., Lentz, R.C.F., McSween, H.Y., Crozaz, G., 2001. A petrologic and trace element study of Dar al Gani 476 and Dar al Gani 489: twin meteorites with affinities to basaltic and lherzolitic shergottites. Meteorit. Planet. Sci. 36, 195–208.
Wang, K., Moynier, F., Dauphas, N., Barrat, J.-A., Craddock, P., Sio, C.K., 2012. Iron isotope fractionation in planetary crusts. Geochim. Cosmochim. Acta 89, 31–45.
Wang, K., Moynier, F., Barrat, J.-A., Zanda, B., Paniello, R.C., Savage, P.S., 2013. Homogeneous distribution of Fe isotopes in the early solar nebula. Meteorit. Planet. Sci. 48, 354–364.
Wang, K., Jacobsen, S.B., Sedaghatpour, F., Chen, H., Korotev, R.L., 2015. The earliest Lunar Magma Ocean differentiation recorded in Fe isotopes. Earth Planet. Sci. Lett. 430, 202–208.
Wanke, H., Dreibus, G., 1988. Chemical composition and accretion history of terrestrial planets. Philos. Trans. R. Soc. A, Math. Phys. Eng. Sci. 325, 545–557.
Wasson, J.T., Kallemeyn, G.W., 1988. Compositions of chondrites. Philos. Trans. R. Soc. A, Math. Phys. Eng. Sci. 325, 535–544.
Weyer, S., Ionov, D.A., 2007. Partial melting and melt percolation in the mantle: the message from Fe isotopes. Earth Planet. Sci. Lett. 259, 119–133.
Weyer, S., Anbar, A., Brey, G., Munker, C., Mezger, K., Woodland, A., 2005. Iron isotope fractionation during planetary differentiation. Earth Planet. Sci. Lett. 240, 251–264.
Williams, H.M., Wood, B.J., Wade, J., Frost, D.J., Tuff, J., 2012. Isotopic evidence for internal oxidation of the Earth's mantle during accretion. Earth Planet. Sci. Lett. 321–322, 54–63.
Wood, B.J., Walter, M.J., Wade, J., 2006. Accretion of the Earth and segregation of its core. Nature 441, 825–833.
Zambardi, T., Poitrasson, F., Corgne, A., Méheut, M., Quitté, G., Anand, M., 2013. Silicon isotope variations in the inner solar system: implications for planetary formation, differentiation and composition. Geochim. Cosmochim. Acta 121, 67–83.
Zhang, J., Dauphas, N., Davis, A.M., Leya, I., Fedkin, A., 2012. The proto-Earth as a significant source of lunar material. Nat. Geosci. 5, 251–255.
Zhao, X., Zhang, H., Zhu, X., Tang, S., Yan, B., 2012. Iron isotope evidence for multistage melt–peridotite interactions in the lithospheric mantle of eastern China. Chem. Geol. 292, 127–139.